Optics Letters

Amplitude-phase optimized long depth of focus femtosecond axilens beam for single-exposure fabrication of high-aspect-ratio microstructures

Deng Pan,[1] Bing Xu,[1] Shunli Liu,[1] Jiawen Li,[1,2] Yanlei Hu,[1] Dong Wu,[1,3] and Jiaru Chu[1]

[1]CAS Key Laboratory of Mechanical Behavior and Design of Materials, Department of Precision Machinery and Precision Instrumentation, University of Science and Technology of China, Hefei 230026, China
[2]e-mail: jwl@ustc.edu.cn
[3]e-mail: dongwu@ustc.edu.cn

Received 6 February 2020; revised 3 March 2020; accepted 15 March 2020; posted 16 March 2020 (Doc. ID 389946); published 28 April 2020

Fabrication of high-aspect-ratio (HAR) micro/nanostructures by two-photon polymerization (TPP) has become a hot topic because of the advantages of ultra-high resolution and true 3D printing ability. However, the low efficiency caused by point-by-point scanning strategy limits its application. In this Letter, we propose a strategy for the rapid fabrication of HAR microstructures by combining TPP with an amplitude-phase optimized long depth of focus laser beam (LDFB). The optimization of the LDFB is implemented by modulating the amplitude and phase on a phase-only spatial light modulator, which can suppress the side lobe and smooth energy oscillations effectively. The LDFB is used for rapid fabrication of HAR micropillars and various microstructures, which greatly increases the fabrication efficiency. As a demonstration, several typical HAR microstructures such as assemblies, microchannels, microtubes, and cell scaffolds are prepared. Moreover, the microcapture arrays are rapidly fabricated for the capture of microspheres and the formation of microlens arrays, which show focusing and imaging ability.

https://doi.org/10.1364/OL.389946

High-aspect-ratio (HAR) micro/nanostructures have attracted great attention due to their broad applications in microoptics, micromechanics, microbiology, and so on [1–3]. Correspondingly, a variety of manufacturing techniques have been developed, including deep silicon etching, nanoimprinting, and UV printing [4–6]. Among these methods, two-photon polymerization (TPP) is a promising method with the advantages of high resolution, true 3D printing ability, and flexibility [7,8]. Nevertheless, a conventional TPP system is based on a point-by-point scanning strategy and consumes a great deal of processing time. The low processing efficiency of TPP has become a key factor limiting its application. An alternative way to solve this problem is to introduce the spatial light modulator (SLM) into a 2PP processing system that can modulate the phase of the femtosecond laser beam and adjust the shape of the laser beam. Hence, the point-by-point scanning is changed into layer-by-layer or even voxel-by-voxel exposure, leading to greatly improved fabrication efficiency [9,10]. A variety of complex shaped beams such as double-helix beams, vortex beams, and Bessel beams have been realized for the rapid fabrication of numerous functional microstructures [11–13]. Until now, all of these have focused on various complex shaped beams for rapidly fabricating large-area 2D-3D microstructures. The potential of using shaped beams to fabricate HAR microstructures has not been fully exploited.

A long depth of focus laser beam (LDFB), such as a Bessel beam, has the advantages of high resolution and long focal length, and is widely used in optical imaging, optical tweezers, and optical processing [14–17]. However, due to the light propagation in a straight line and the conservation of the beam energy, it will be inevitably accompanied by an axial or radial light field oscillation when a LDFB is generated. These undesired oscillations cause various negative effects. For example, radial light field oscillations can cause annular defects or axial point defects around holes when drilling with a Bessel beam [18,19]. The signal-to-noise ratio is not ideal when imaging with a Bessel beam due to the interference of the beam oscillation [20,21]. These oscillations limit the application of a LDFB in optical processing. Several techniques have been reported for smoothing the LDFB oscillation and improving the energy utilization rate. For example, Davidson *et al.* [22] and Sochacki *et al.* [23,24] modulated the light wavefront of Bessel beams to a quadric surface or a logarithmic surface, and introduced the variable of the surface slope to control the beam intensity distribution. Another method to improve the uniformity of the LDFB is to apodize the phase, which can control the starting and ending positions of the LDFB. Nevertheless, the sudden change of the phase will cause a sharp oscillation in the axial direction. Jaroszewicz *et al.* smoothed this oscillation by introducing amplitude modulation of the LDFB [25], but this method is difficult to implement in a phase-only SLM-assisted TPP system.

In this work, we apply amplitude and phase modulation on a phase-only SLM simultaneously to smooth the axial and radial oscillations of LDFB. Combined with a TPP single point scanning system, HAR micropillars can be processed with one-step exposure. This method can fabricate the HAR microstructures/microdevices in a short time, which greatly improves the processing efficiency. As a demonstration, we performed rapid processing of the microcapture arrays, and realized the capture of microspheres and the generation of microlens arrays.

The phase of the LDFB can be written as

$$\varphi(r) = -\frac{R^2(Z_1+Z_2)}{2Z_2^2} * \ln\left[\frac{Z_1 Z_2}{Z_1+Z_2} + \frac{Z_2^2}{R^2(Z_1+Z_2)} r^2\right], \tag{1}$$

where R is the radius of the diffraction plane and Z_1/Z_2 are the beginning and end positions of the LDFB. The LDFB is a kind of axilens beam, and is similar to a Bessel beam. The wavefront shape of a LDFB is a logarithmic-curved shape, while the wavefront shape of a Bessel beam is an isosceles triangle shape, which means that another parameter (curvature) can be introduced for the flexible modulation of Z_1 and Z_2. The holograms can be obtained by computing Formula 1, and the results are shown in Fig. 1(a-1) ($Z_1 = 100$ mm and $Z_2 = 400$ mm). Although the LDFB can generate a long depth of focus, the ending position cannot be controlled at the predesigned position (400 mm). Moreover, the axial light intensity distribution is uneven, and the light intensity at the beginning is about two times higher than the intensity at the middle and end positions [Fig. 1(c)]. To solve this problem, an aperture is used to apodize the phase, and the $\varphi(r)$ is limited by RZ_1/Z_1 and R [Fig. 1(a-2)]. Due to the introduction of apodization, the beam position can be precisely controlled between 100 and 400 mm [Fig. 1(d)]. However, the sharp changes of phase caused by the apodization result in rapid light intensity oscillations in the axial direction. For smoothing these oscillations, an alternative method is to apply smooth apodization by amplitude modulation. The amplitude transmittance function can be written as

$$A(r) = \begin{cases} 0 & 0 < r < r_1 \\ \sin^2\left[\dfrac{\pi Z_2^2\left(r^2 - \frac{R^2 Z_1^2}{Z_2^2}\right)}{2R^2(Z_1+Z_2)\Delta}\right] & r_1 < r < r_2 \\ 1 & r_2 < r < r_3 \\ \sin^2\left[\dfrac{\pi Z_2^2(R^2-r^2)}{2R^2(Z_1+Z_2)\Delta}\right] & r_3 < r < R \end{cases}, \tag{2}$$

where $r_1 = \frac{RZ_1}{Z_2}$, $r_2 = \frac{RZ_1}{Z_2}\left(1 + \frac{Z_1+Z_2}{Z_1^2}\Delta\right)^{0.5}$, $r_3 = R\left(1 - \frac{Z_1+Z_2}{Z_2^2}\Delta\right)^{0.5}$, and Δ is the small fraction of the region. Due to the introduction of the amplitude transition zone, the oscillation of the light intensity is well suppressed. Here, $\Delta = 0$ corresponds to apodization without smoothing [Fig. 1(d)]. As Δ becomes larger, the light intensity becomes smoother or even excessively smoother, causing the light intensity to concentrate in the middle [Fig. 1(b)]. Therefore, it is critical to choose a suitable Δ for a specific situation. For example, when $Z_1 = 100$ mm and $Z_2 = 400$ mm, Δ can be given as 50 mm, which can effectively suppress the oscillation without making the beam excessively concentrated [Figs. 1(a-3) and 1(e)].

In this optimization method, amplitude modulation is used to optimize the LDFB intensity distribution. However, in a conventional TPP system, the commonly used SLM is a phase-only liquid crystal SLM. Therefore, phase coding is needed. Until now, there have been reports about the complex spatial modulation on a phase-only SLM [26–28]. Here, the blazed grating (BG) is used to encode the amplitude information. As shown in Fig. 2(a), the BG with period T not only can separate the +1st order light from the 0th order, but also can be used to adjust the diffraction efficiency of each order. The diffraction efficiency η can be written as

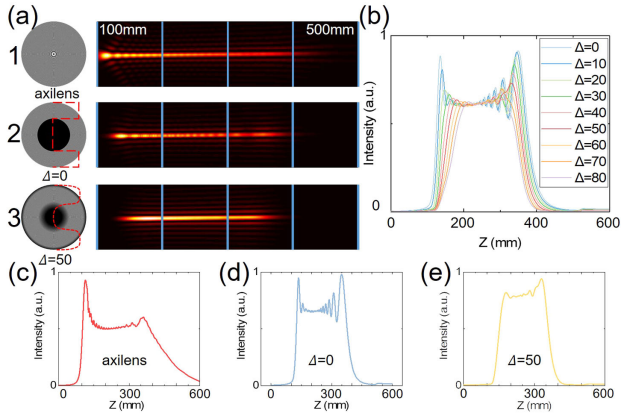

Fig. 1. Optimization of LDFB. (a) Axial intensity distribution of (a-1) axilens beam, (a-2) phase optimized axilens beam, and (a-3) amplitude-phase optimized axilens beam. (b) Intensity axial distribution under different Δ. (c)–(e) Axial intensity of axilens beam, phase optimized axilens beam, and amplitude optimization of light.

$$\eta(\varphi) = \frac{2(1-\cos\varphi)}{(\varphi - 2m\pi)^2}, \tag{3}$$

where m is the diffraction order, and φ is the modulation depth. As $\varphi = 2\pi$, all the light is diffracted into the +1st order. However, when the φ decreases, part of the light is diffracted into the 0th order and −1st order, resulting in the decreased 1st order light diffraction efficiency [Fig. 2(c)]. Therefore, the amplitude modulation can be realized on a phase-only SLM by coding the modulation depth of BG according to the amplitude transmittance function [Fig. 2(b)]. The complex amplitude of LDFB can be written as

$$U(r) = A(r)\exp(\varphi(r) + 2\pi x/T). \tag{4}$$

It can be considered that the diffraction efficiency is the intensity of the emitted light. Hence, it has the following relationship:

$$a(r) = \eta^{-1}(A(r)), \tag{5}$$

where $a(r)$ is the encoding phase corresponding to the amplitude transmittance function $A(r)$. Therefore, the coded complex amplitude of LDFB is

$$U(r) = \exp(\mathrm{mod}(\varphi(r) + 2\pi x/T, 2\pi)a(r)). \tag{6}$$

In order to introduce the LDFB for TPP, a typical femtosecond laser (central wavelength of 800 nm; repetition rate of 80 MHz; pulse width of 75 fs) TPP system combined with a phase-only SLM (Holoeye, 1920 × 1080) is used [Fig. 2(a)]. After expansion by the beam expander, the laser beam is reflected

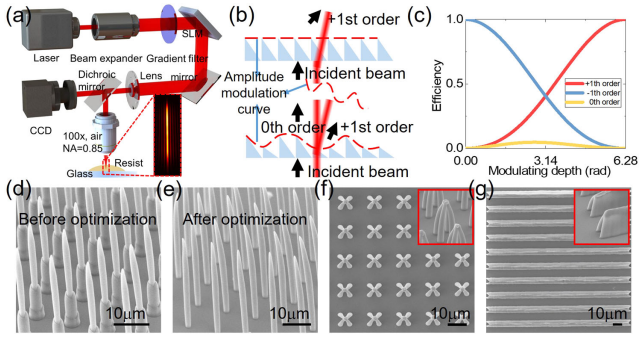

Fig. 2. Realization of amplitude-phase modulation on a pure phase SLM. (a) Diagram of TPP system. (b) Schematic of modulation of light amplitude by a blazed grating. (c) Diffraction efficiency of different modulation depth and different diffraction order beam. (d) Side-lobe microstructures exposed by the unoptimized axilens beams. (e) Prefect HAR micropillars fabricated by one-step exposure. (f) Top view and side view of four-micropillar assemblies. (g) Top view and side view of self-assembled microtubes.

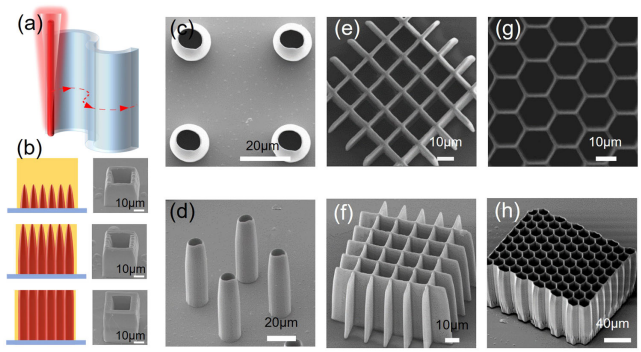

Fig. 3. Using the optimized axilens beam to fabricate HAR microstructures/microdevices by line scanning. (a) Schematic of single scanning processing. (b) Surface quality of the microstructure is improved with increasing processing depth. (c) and (d) Top view and side view of microtubes fabricated by single scanning exposure. (e) and (f) Top view and 45° view of common shape cell scaffold. (g) and (h) Top view and 45° view of orthogonal hexagonal liver cell scaffold.

by the SLM, and the laser beam energy is controlled by a gradient filter. A 4f system composed of a lens ($f = 200$ mm) and an objective lens (air, 100×, NA = 0.85) is adopted to reconstruct the LDFB under the objective lens. After exposure by the LDFB, the photoresist (SZ2080) is soaked with n-propanol to remove the unprocessed areas and dried with a CO_2 critical point dryer to avoid the capillary force. To compare the effects before and after the amplitude optimization, the holograms in Figs. 1(a-1) and 1(a-3) are used to fabricate a HAR microstructure under the same conditions (exposure time of 10 ms, laser energy of 200 mW). The microstructures exposed by the unoptimized LDFB have significant side-lobe structures, while the optimized LDFB can fabricate a prefect HAR micropillar by one-step exposure, which proves that this optimized method can effectively suppress the appearance of side lobes and oscillation of the LDFB, as shown in Figs. 2(d) and 2(e). Using this method, one-step exposure can fabricate a HAR micropillar (height of 50 μm and diameter of 2 μm). Interestingly, if the micropillars are dried under natural volatile conditions, four micropillars can self-assemble to form a stable, flower-like microstructure [Fig. 2(f)]. Furthermore, if the single point exposure strategy is changed to a line-scanning exposure strategy, the microwalls can be fabricated at a rapid speed (2 s for a microwall with 100 μm length and 15 μm height), which improves the fabrication efficiency by about 50 times. The two thin microwalls could assemble into one microchannel when the developer evaporates [Fig. 2(g)]. It is worth noting that the assembled microchannels could be infinitely long within the range permitted by the platform stroke because the unprocessed area is removed ahead of the formation of the microchannels. These microchannels have broad application prospects, including lab-on-a-chip systems, cancerous vessels, cell growth, and tissue engineering.

Except for fabricating the simple HAR micropillars, HAR microstructures and microdevices with complex shapes can also be manufactured through this strategy. As illustrated in Fig. 3(b), the diameter of the LDFB gradually increases with the increase of the propagation distance, but remains consistent in the middle and rear parts. Therefore, we focused the middle and rear segments of the LDFB into the photoresist to obtain a good surface quality. The 45° scanning electron microscope (SEM) images in Fig. 3(b) demonstrate that the surface quality of the microstructure and microdevice becomes better when the relative position between the sample and LDFB changes. No matter how high the microstructure, the time consumption is the same because a single exposure can produce a HAR columnar voxel [Fig. 3(a)]. This means that, within the range of the fabrication capacity, the higher the microstructure, the higher the efficiency. For example, when the microstructure height is 100 μm, the processing time of LDFB is only 2% of the point-by-point method. Figures 3(c) and 3(d) are top- and side-view SEM images of circular microtubes with 20 μm diameter,100 μm height, and 2 μm thickness. A HAR microtube is fabricated by simply scanning a circular path within 1 s. In addition, a square cell scaffold (60 μm height, 100 μm length and width, and 15 μm period)and a hexagonal hepatocyte cell scaffold (80 μm height, 180 μm ∗ 150 μm, and 10 μm period) with a thickness of 2 μm can be fabricated in 10 s and 35 s, respectively [Figs. 3(e)–3(h)]. These kinds of HAR hexagonal micro/nanostructure arrays are helpful in the field of hepatocyte tissue engineering.

As a proof of concept demonstration, this method is used to fabricate microcapture arrays for the capture of microspheres and the formation of microlens arrays. It is noteworthy that a microlens consisting of microsphere can be used in super-resolution imaging. Here, the pyramid-shaped microstructures are adopted as the basic unit for composing the microcapture arrays. The pyramid microstructures have better bending resistance characteristics than the micropillar, which will be more stable during the capture process. Figure 4(c) shows the SEM image of the microstructures used for trapping particles. During capture, the ethanol containing 10 μm diameter SiO_2 microspheres was dropped onto the sample. The height of the microtrapping-structure was designed to be 15 μm for only capturing one particle in one trapping structure. Under the action of gravity and hydrodynamic force, the microparticles naturally settled into the pre-processed microstructure and got trapped. Then the sample was washed in ethanol to remove the uncaptured microparticles. The captured microspheres were more relatively stable compared to the uncaptured ones due to the grasping force provided by the microstructure and substrate.

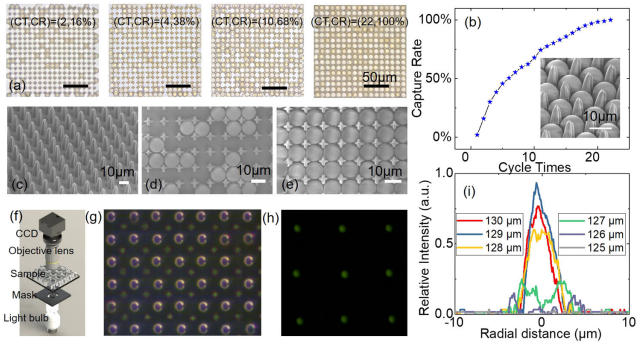

Fig. 4. Formation and characterization of microlens array composed of the captured microspheres. (a) Process of capturing SiO_2 microspheres. (b) Relationship between capture rate and number of cycles. The illustration schematically shows the state when the microsphere is captured. (c) 45° view of capture array. (d) and (e) SEM image of arrays that are not fully filled with small balls and filled with microspheres, respectively. (f) Schematic of test system. (g) Image taken above the microlens array. (h) Spot array obtained by focusing the microlens array. (i) Intensity distribution of the focus of the microlens array at different positions.

As the cycle times (CT) increased, the trapped particles and capture rate (CR) increased [Figs. 4(a) and 4(b)]. Finally, almost all the microtrap structures were filled with microparticles, resulting in the formation of the microlens arrays. Figures 4(d) and 4(e) are the SEM images of the unfilled microstructure and the filled structure, respectively.

To test the imaging effect of the microlens array, the homemade optical system shown in Fig. 4(f) is adpoted. The white light generated by a light bulb is modified by a mask with the letter "C". Afterwards, the modified light is focused and imaged by the sample. Finally, the light intensity distribution at the focal plane is received by an objective lens and caught by the charge-coupled device (CCD). Thanks to the neat arrangement of the microparticles and the close contact between the microparticles and the glass substrate, the periodic "C" pattern can be seen clearly [Fig. 4(g)]. Due to the spherical shape of the microparticle, the parallel light will be converged after passing through the microparticles [Fig. 4(h)]. The focal distance is 129 μm, judging from the statistical distribution of light intensity at different propagation distances [Fig. 4(i)].

In conclusion, we propose a strategy for the rapid fabrication of HAR micropillars and microstructures by combining TPP with amplitude-phase optimized LDFB. The LDFB with uniform light intensity distribution is obtained by modulating the amplitute and phase on a phase-only SLM at the same time and used for one-step exposure of micropillars and microstructures. These high-aspect-ratio micropillars and microwalls can self-assemble into stable, flower-like microstructures and microchannels. Several typical microstructures such as microtubes and cell scaffolds are processed with an efficiency improvement of about 50 to 200 times. As a demonstration, the microcapture arrays are prepared in this way for capturing microspheres, which can form microlens arrays with focusing and imaging ability. We believe that this rapid HAR microstructures process method has promising prospects in the field of microoptics, microfluidics, microbiology, and micromechanics.

Funding. National Key Research and Development Program of China (2017YFB1104303, 2018YFB1105400); National Natural Science Foundation of China (51675503, 51805508, 51805509, 51875544, 61475149, 61805230); Fundamental Research Funds for the Central Universities (WK2090090012, WK2090090021, WK2480000002, WK6030000103, WK6030000131); China Postdoctoral Science Foundation (2019M662190).

Acknowledgment. We acknowledge the Experimental Center of Engineering and Material Sciences at USTC for the fabrication and measuring of samples. This work was partly carried out at the USTC Center for Micro and Nanoscale Research and Fabrication.

Disclosures. The authors declare no conflicts of interest.

REFERENCES

1. P. Du, X. Zheng, I. K. Lin, and X. Zhang, Appl. Phys. Lett. **99**, 083701 (2011).
2. S. Buzzi, M. Galli, M. Agio, and J. F. Löffler, Appl. Phys. Lett. **94**, 223115 (2009).
3. Z. Wang, ACS Nano **12**, 1273 (2018).
4. S. H. Ko, I. Park, H. Pan, C. P. Grigoropoulos, A. P. Pisano, C. K. Luscombe, and J. M. Frechet, Nano Lett. **7**, 1869 (2007).
5. S. Ghosh and G. K. Ananthasuresh, Sci. Rep. **6**, 18428 (2016).
6. M. T. Ghoneim and M. M. Hussain, Small **13**, 1601801 (2017).
7. K. Obata, A. El-Tamer, L. Koch, U. Hinze, and B. N. Chichkov, Light Sci. Appl. **2**, e116 (2013).
8. S. Lightman, G. Hurvitz, R. Gvishi, and A. Arie, Optica **4**, 605 (2017).
9. C. Zhang, Y. Hu, J. Li, Z. Lao, B. Xu, J. Ni, Z. Cai, D. Wu, and J. Chu, Opt. Eng. **55**, 035102 (2016).
10. D. Yang, L. Liu, Q. Gong, and Y. Li, Macromol. Rapid Commun. **40**, 1900041 (2019).
11. S.-J. Zhang, Y. Li, Z.-P. Liu, J.-L. Ren, Y.-F. Xiao, H. Yang, and Q. Gong, Appl. Phys. Lett. **105**, 061101 (2014).
12. L. Yang, D. Qian, C. Xin, Z. Hu, S. Ji, D. Wu, Y. Hu, J. Li, W. Huang, and J. Chu, Appl. Phys. Lett. **110**, 221103 (2017).
13. S. Ji, L. Yang, C. Zhang, Z. Cai, Y. Hu, J. Li, D. Wu, and J. Chu, Opt. Lett. **43**, 3514 (2018).
14. S. Ahlawat, R. S. Verma, R. Dasgupta, and P. K. Gupta, Appl. Opt. **50**, 1933 (2011).
15. C. Shen, Q. Hong, Q. Zhu, C. Zu, and S. Wei, Opt. Laser Technol. **120**, 105682 (2019).
16. Z. Yao, L. Jiang, X. Li, A. Wang, Z. Wang, M. Li, and Y. Lu, Opt. Express **26**, 21960 (2018).
17. D. Pan, S. Liu, S. Ji, Z. Cai, J. Li, Y. Hou, W. Zhang, S. Fan, R. Li, Y. Hu, W. Zhu, D. Wu, and J. Chu, Opt. Lett. **45**, 897 (2020).
18. F. He, J. Yu, Y. Tan, W. Chu, C. Zhou, Y. Cheng, and K. Sugioka, Sci. Rep. **7**, 40785 (2017).
19. Z. Wang, L. Jiang, X. Li, A. Wang, Z. Yao, K. Zhang, and Y. Lu, Opt. Lett. **43**, 98 (2017).
20. W. Yu, Z. Ji, D. Dong, X. Yang, Y. Xiao, Q. Gong, P. Xi, and K. Shi, Laser Photon. Rev. **10**, 147 (2016).
21. L. Gao, L. Shao, B. C. Chen, and E. Betzig, Nat. Protoc. **9**, 1083 (2014).
22. N. Davidson, A. A. Friesem, and E. Hasman, Opt. Lett. **16**, 523 (1991).
23. J. Sochacki, S. Bara, Z. Jaroszewicz, and A. Kolodziejczyk, Opt. Lett. **17**, 7 (1992).
24. J. Sochacki, A. Kolodziejczyk, Z. Jaroszewicz, and S. Bara, Appl. Opt. **31**, 5326 (1992).
25. Z. Jaroszewicz, J. Sochacki, A. Kolodziejczyk, and L. R. Staronski, Opt. Lett. **18**, 1893 (1993).
26. J. A. Davis, D. M. Cottrell, J. Campos, M. J. Yzuel, and I. Moreno, Appl. Opt. **38**, 5004 (1999).
27. I. Rincon and V. Arrizon, OSA Continuum **2**, 2983 (2019).
28. R. W. Cohn and M. J. A. O. Liang, Appl. Opt. **33**, 4406 (1994).